Enhanced Seebeck coefficient through energy-barrier scattering in PbTe nanocomposites

J. Martin,[1] Li Wang,[2] Lidong Chen,[2] and G. S. Nolas[1,*]
[1]*Department of Physics, University of South Florida, Tampa, Florida 33620, USA*
[2]*State Key Laboratory of High Performance Ceramics and Superfine Microstructures, Shanghai Institute of Ceramics, Chinese Academy of Sciences, Shanghai 200050, China*
(Received 1 August 2008; published 13 March 2009)

Resistivity, Seebeck coefficient, and Hall measurements were performed on densified nanocrystalline composite materials of undoped and Ag-doped PbTe nanocrystals to investigate the physical mechanisms responsible for Seebeck coefficient enhancement in nanocrystalline systems. The unique temperature dependence of the resistivity and mobility for these PbTe nanocomposites suggests that grain-boundary potential barrier scattering is the dominant scattering mechanism. We propose that carrier trapping in the grain boundaries forms energy barriers that impede the conduction of carriers between grains, essentially filtering charge carriers with energy less than the barrier height. These nanocomposites therefore demonstrate an enhanced Seebeck coefficient as compared to single crystal or polycrystalline PbTe at similar carrier concentrations.

DOI: 10.1103/PhysRevB.79.115311 PACS number(s): 73.63.−b, 72.15.Jf

I. INTRODUCTION

The controlled fabrication of nanoscale semiconductors with enhanced physical properties is a current goal of technical as well as fundamental interest. To this end, the influence of semiconductor grain boundaries on carrier transport becomes increasingly important in nanoscale polycrystalline systems, where surface, point defect, dislocation, and interfacial energy barrier scatterings can dominate the transport.[1–3] Recent identification of several higher efficiency thermoelectric (TE) materials can be attributed to nanoscale enhancement.[4–11] These materials demonstrate increased Seebeck coefficient and decreased thermal conductivity due to the phenomenological properties of nanometer length scales, including enhanced interfacial phonon scattering and charge carrier filtering. Nanostructured TE enhancement aims to "split" the interdependence of the electrical and thermal transport, allowing for better optimization of the TE figure of merit, $ZT=S^2T/\rho\kappa$.[12] This equation defines the effectiveness of a material for TE applications, where S is the Seebeck coefficient, T is the absolute temperature, ρ is the electrical resistivity, and κ is the thermal conductivity. The reduction in κ through the interface scattering of phonons remains the primary mechanism for increased TE performance in nanostructured systems.[4,6–8] However, to achieve superior TE performance requires enhancement of the power factor (S^2/ρ). Carrier filtering, where the presence of interfacial energy barriers filters low-energy charge carriers traversing the interface, has been theoretically predicted.[13,14] This increases $|S|$, as its value depends on the mean carrier energy relative to the Fermi level.[12] An understanding of this phenomenon in bulk materials is of fundamental importance. A small body of work has indicated that TE property improvements for bulk nanocrystalline materials are feasible;[15–17] however, the physical mechanism responsible for S enhancement in these materials has not been developed. To this end, we investigate the transport properties of doped and undoped nanocomposites, i.e., nanocrystals densified within a macroscale nanocomposite, in order to promote further insight and stimulate fundamental research into the transport of polycrystalline bulk semiconductor grain boundaries.

II. RESULTS AND DISCUSSION

PbTe nanocomposites were prepared by densifying 100 nm PbTe nanocrystals synthesized in high-yield employing a solution-phase reaction of two monometallic aqueous precursor solutions.[17,18] The carrier concentrations were modified by directly doping the PbTe nanocrystals with Ag (Ag_2Te) prior to the densification procedure (specimens III and IV). Spark plasma sintering (SPS) successfully consolidated these nanoscale grains within a dense PbTe matrix at 95% bulk theoretical density. As we have previously shown,[17] densifying solely the nanocrystals results in the dispersion of nonconglomerated nanostructure within a bulk matrix, with grains ranging from 100 nm to over 1 μm. Table I lists room-temperature physical properties, described below. X-ray diffraction following SPS indicated ~5 vol % $PbTeO_3$ impurity for specimens I and II, and ~3 vol % TeO_2 impurity for specimens III and IV.

The nanocomposites were cut into $2\times2\times5$ mm^3 parallelepipeds for transport property measurements. Four-probe ρ and S were measured from 12 to 300 K in a custom radiation-shielded vacuum probe with maximum uncertainties of 4% and 6%, respectively, at 300 K.[19] Temperature-dependent four-probe Hall measurements were conducted from 5 to 300 K at both positive and negative magnetic fields of up to 5 T to eliminate voltage probe misalignment effects.

For all specimens, a linear and positive magnetic field dependence of the Hall resistance confirms dominant p-type conduction. The carrier concentrations increase upon Ag doping by more than a factor of 5, as listed in Table I. Correspondingly, the ρ values, as shown in Fig. 1, exhibit a significant reduction in magnitude compared to the undoped specimens. All specimens exhibit relatively large room-temperature S values of approximately 325 μV/K for the two undoped specimens and 200 μV/K for the two Ag-doped specimens.

TABLE I. Room temperature thermal conductivity κ, resistivity ρ, Seebeck coefficient S, carrier concentration p, energy barrier height E_B, trapping state density N_t, energy barrier width W, and effective crystallite size L, at 300 K, for undoped PbTe (specimens I and II) and Ag-doped PbTe (specimens III and IV).

Specimen	κ (W m^{-1} K^{-1})	ρ (mΩ cm)	S (μV/K)	p (cm^{-3})	E_B (meV)	N_t (cm^{-2})	W (nm)	L (nm)
I	2.2	24.9	328	9.5×10^{17}	60	1.0×10^{13}	54	316
II	2.5	12.6	324	1.5×10^{18}	60	1.3×10^{13}	43	396
III	2.8	3.9	198	5.1×10^{18}	60	2.4×10^{13}	23	376
IV	2.7	2.9	207	6.2×10^{18}	60	2.6×10^{13}	21	416

The low-temperature ρ values show activated temperature dependence ($d\rho/dT<0$) in all specimens and a nonlinear increase with decreasing temperature but with a sharp peak in ρ near 70 K for the Ag-doped specimens (Fig. 1). Below 70 K the ρ values rapidly decrease with decreasing temperature. However, temperature-dependent carrier concentration for all specimens indicates only a weak dependence with temperature. Lead chalcogenides exhibit large dielectric permittivity (ε) and small effective mass (m^*) that merge impurity levels with the allowed energy band, resulting in low-temperature impurity ionization, with energy $\propto m^*\varepsilon^{-2}$.[20–22] Consequently, the carrier concentration remains approximately constant where there is no degeneracy down to low temperature.

Figure 2 shows the temperature dependence of the mobility, μ, for the two Ag-doped specimens in comparison to the two undoped nanocomposites. While the room temperature mobilities are consistent with those reported in the literature, the temperature dependence differs significantly from single crystal and polycrystalline lead chalcogenides since the nanocomposite mobilities decrease with decreasing temperature, opposite to that of bulk materials reported in the literature.[20–24] In addition, the low-temperature μ values for the Ag-doped specimens also show an order of magnitude increase as compared to the undoped specimens and exhibit a dip in μ (an approximately twofold decrease) near 80 K, as compared to those values at the lowest temperature.

The scattering mechanisms that dominate the transport in bulk lead chalcogenides do not fully describe the unique temperature dependence of μ in these nanocomposites, implying the presence of an additional scattering mechanism. In nondegenerate semiconductors the carriers are scattered by long-wavelength acoustic phonons, $\mu\propto m^{*-5/2}T^{-3/2}$.[20] Since the factor $m^{*-5/2}$ is inversely proportional to temperature in lead chalcogenides (based on experimental temperature dependence of m^*), the mobility therefore varies with $T^{-5/2}$, as experimentally observed in single crystal and polycrystalline lead chalcogenides, with a weaker dependence on degenerate specimens.[20,21] This dependence is opposite of that observed in the PbTe nanocomposites, suggesting that phonon scattering is present in combination with an additional mechanism. Furthermore, the experimental data indicate that μ is not proportional to $T^{3/2}$ in these nanocomposites and suggests scattering by ionized impurities is not a dominant mechanism. The high ε in PbTe implies suppression of long-range Coulomb potentials, limiting scattering to near the internal point of an impurity due to the large Bohr radius ($\propto m^{*-1}\varepsilon$, on the order of the lattice constant),[25,26] and consequently, a small screening length. Therefore, it is unlikely that ionized impurity scattering is effectively present in these nanocomposites, particularly at room temperature where the interaction time (the time required for the carrier to pass the region of one impurity ion)[26] is significantly shorter.

The nanocomposite carrier conduction can be effectively described as dominated by grain-boundary potential barrier

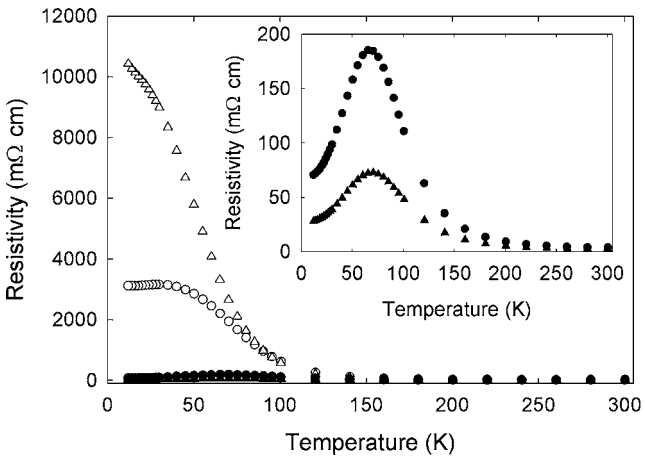

FIG. 1. Temperature dependence of the resistivity for specimens I (○), II (△), III (●), and IV (▲).

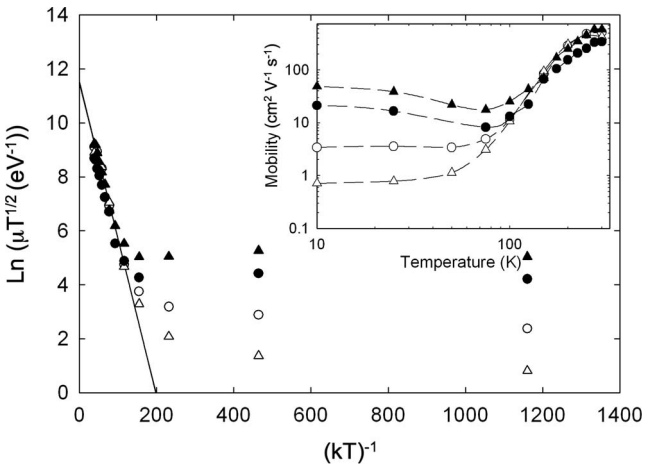

FIG. 2. Temperature dependence of the mobility for specimens I (○), II (△), III (●), and IV (▲). Lines are a guide for the eye only. Plotting the logarithm of $\mu_{\text{eff}}=\mu_0(1/T)^{1/2}\exp(-E_B/kT)$ and fitting the high-temperature data yields an energy barrier of 60 meV for all specimens.

scattering, in combination with phonon scattering. Similar models have successfully described the electrical properties of silicon, CdTe, and nanostructured metal oxide films.[3,27–29] Our previous work indicated oxygen adsorption in the PbTe nanocomposites.[17] This surface reactivity is difficult to prevent, considering the aqueous nature of the synthesis technique.[17,18] The surface oxidation of PbTe is a sequential process, proceeding first through the formation of weak peroxidelike structures (up to 70% coverage) then by the chemisorption of oxygen.[30] Density-functional theory calculations of the surface reactivity of PbTe (Ref. 30) indicate that these oxygen complexes form chemical bonds by transferring charge from the tellurium atoms.[30] These chemical shifts were experimentally confirmed through x-ray photoemission spectroscopy.[30] The chemisorption of oxygen essentially forms carrier trapping acceptor states by removing electrons from the grain surface, reducing itinerant carrier density. For nanocrystalline materials, this chemisorption results in increased trapping of carriers at grain boundaries, forming energy barriers that impede the conduction of carriers between grains. Assuming a uniformly distributed concentration of ionized carrier traps, N_t/cm^2, a grain-boundary thickness less than the crystallite size L, whose morphology and size distribution are identical, and ρ within the grains less than through the boundary, the effective mobility is given by[27]

$$\mu_{\mathrm{eff}} = Lq\left(\frac{1}{2\pi m^* kT}\right)^{1/2} \exp\left(-\frac{E_B}{kT}\right), \tag{1}$$

where q is the carrier charge, m^* is the effective mass, k is the Boltzmann constant, T is the temperature, and E_B is the height of the energy barrier in the depletion region. A plot of the logarithm of μ vs $1/kT$ for the PbTe nanocomposites indicates activated behavior from conduction through the boundary potential barrier between grains (Fig. 2). Fitting the higher-temperature data yields an energy barrier $E_B = 60$ meV for all specimens. This suggests the energy barriers form through a similar oxygen chemisorption mechanism in both the undoped and Ag-doped specimens. Conduction through ballistic transport occurs when the average energy of the charge carriers is sufficient to overcome this energy barrier. As the temperature increases, the average energy of the charge carriers increases and therefore the electrical conductivity increases $\propto T^{-1/2} \exp(-E_B/kT)$. This mechanism dominates at higher temperature and for higher carrier densities, where the concentration of carriers with larger average energy is larger. However, an additional conduction mechanism dominates at lower temperature. When the grain-boundary energy barrier is sufficiently narrow and high, the charge carriers quantum mechanically tunnel through the barrier.[27] In equilibrium, the dependence of barrier height E_B on the density of trapping states N_t and the carrier concentration p is given by[3,28] $E_B = q^2 N_t^2 / 8\varepsilon\varepsilon_0 p$, and the barrier width (space charge region) by $W = (2\varepsilon\varepsilon_0 E_B / q^2 p)^{1/2}$, where q is the carrier charge, $\varepsilon = 414$ for PbTe at 300 K,[31] and ε_0 is the vacuum permittivity. Table I lists these calculated values for the two undoped specimens in comparison to the two Ag-doped specimens. As the carrier concentration increases with doping, the barrier height remains constant but promotes an increase in trapping state density. Furthermore, as the carrier concentration increases, the barrier width decreases by a factor $\propto p^{-1/2}$. This suggests an increase in tunneling conduction (transmission probability) with doping.

The one-dimensional time-independent WKB transmission probability τ for the potential barrier is given by[32]

$$\tau(E) = \exp\left(-2\int_{x_1}^{x_2} \{2m^*[qV(x) - E]\}^{1/2} dx/\hbar\right), \tag{2}$$

where x_1 and x_2 are the classical carrier turning points with energy E, m^* is the effective mass, and $qV(x)$ is the interfacial barrier energy. Therefore, the tunneling probability is a maximum for charge carriers with smaller m^*. The electrical transport in p-type PbTe is dominated by two bands: a lower mobility heavy-hole (HH) valence band below the light-hole (LH) valence band at low temperature, where $10m_{\mathrm{LH}}^* \sim m_{\mathrm{HH}}^*$.[20,33] We assume similar m^* and band structure for the nanocomposites. At low temperature and higher hole densities, the electrical properties are dominated nearly exclusively by the LH carriers. As the temperature increases, the HH band rises, resulting in a decreasing τ and an increase in carrier scattering for the higher carrier density specimens. At higher temperature, when the average energy of the charge carriers is sufficient to overcome the grain-boundary energy barrier, conduction is dominated through thermionic emission, $T^{1/2} \exp(-E_B/kT)$, and μ increases with temperature. Grain-boundary potential barrier scattering of the carriers, in combination with phonon scattering, gives rise to the unique temperature dependence of the electrical conductivity and the mobility in these nanocomposites.

The effective crystallite size was estimated using Eq. (1), the energy barriers obtained from fitting the temperature dependence of μ, the μ values calculated from the room temperature carrier concentration, and the HH $m^* = 1.5m_0$.[20] These estimates indicate effective crystallite sizes between 300 and 400 nm, listed in Table I, and are consistent with the dimensional nanocomposite structure observed in our scanning electron microscopy analyses. This suggests the grain-boundary energy barrier scattering is dominated through these nanoscale features. We note that inclusion of LH carriers in the calculation would only slightly lower the effective crystallite size.

Furthermore, conduction through the boundary potential barrier between grains essentially filters lower-energy charge carriers, increasing the average carrier energy and consequently, $|S|$. Figure 3 shows the room temperature S for the PbTe nanocomposites in comparison to theoretically calculated bulk values,[20,34] indicating an enhancement in S as compared to bulk PbTe at the same carrier concentration. In addition, we compare the room temperature S^2/ρ for the nanocomposites to two of our undoped and two Na-doped bulk PbTe specimens, indicating an enhancement in S^2/ρ over that of bulk PbTe by up to a factor of 2 (inset in Fig. 3). The larger S^2/ρ in the nanocomposites as compared to bulk polycrystalline materials, in addition to similar thermal conductivities (Table I and Ref. 20), results in enhanced room-temperature ZT of up to a factor of 2 as compared to bulk PbTe. This suggests that interfacial energy barrier carrier fil-

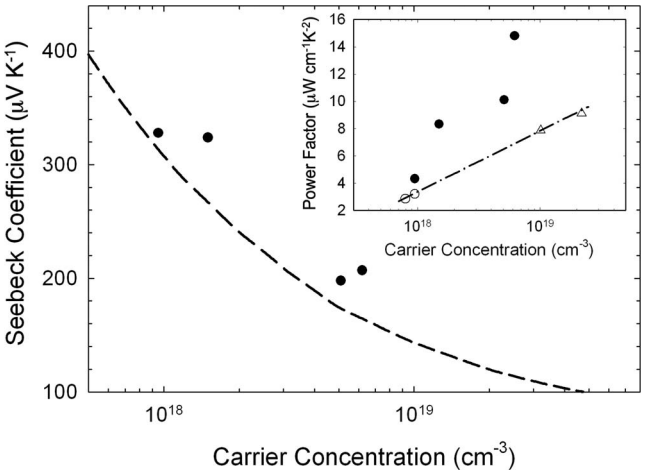

FIG. 3. Room-temperature Seebeck coefficient as a function of carrier concentration for the four PbTe nanocomposites (●) and the calculated bulk relationship (dashed line) from Ref. 34. Inset: room-temperature power factor as a function of carrier concentration for the four PbTe nanocomposites in comparison to bulk undoped PbTe (○) and Na-doped PbTe (△). The straight line is a guide for the eye only.

tering may be an effective method of thermoelectric performance enhancement in these bulk nanocomposites. Similar carrier filtering enhancements to *S* were observed in InGaAs/InGaAlAs heterostructures.[35] We note that interfacial energy barrier carrier filtering may not require nanoscale features (or grain-boundary oxide formation), and similar activated conduction could, to some degree, be observed in bulk polycrystalline chalcogenide systems prepared in nonreducing atmospheres. However, nanoscale features increase the density of these interfaces, thereby enhancing the effective filtering.

III. CONCLUSION

In conclusion, PbTe nanocomposites were prepared by densifying 100 nm PbTe nanocrystals synthesized in high yield employing a solution-phase technique. SPS successfully consolidated these nanoscale grains within a dense PbTe matrix. The carrier concentrations were modified by directly doping the PbTe nanocrystals with Ag prior to densification. The unique temperature dependence of ρ and μ suggests an additional scattering mechanism in combination with phonon-carrier scattering dominant in single crystal and polycrystalline lead chalcogenides. For these nanocrystalline materials, we suggest that the chemisorption of oxygen may result in increased trapping of carriers at grain boundaries, forming energy barriers that impede the conduction of carriers between grains. This conduction can be effectively described as dominated by grain-boundary potential barrier scattering, in combination with phonon scattering. Furthermore, these nanocomposites demonstrate an enhanced TE performance as compared to bulk PbTe, suggesting that interfacial energy barrier carrier scattering is an effective method of thermoelectric performance enhancement in bulk nanocomposites.

ACKNOWLEDGMENTS

G.S.N. and J.M. were supported by the U.S. Army Medical Research and Materiel Command under Grant No. W81XWH-07-1-0708 and the University of South Florida Functional Materials and Manufacturing by Design (FMMD) project. J.M. and G.S.N. thank L. Woods and A. Popescu at USF and J. Yang at General Motors for insightful conversations. Additionally, the authors thank J. Salvador of General Motors for Hall measurements.

*gnolas@cas.usf.edu

[1] G. Blatter and F. Greuter, Phys. Rev. B **34**, 8555 (1986).
[2] H. Marom, M. Ritterband, and M. Eizenberg, Thin Solid Films **510**, 62 (2006).
[3] C. H. Seager, J. Appl. Phys. **52**, 3960 (1981).
[4] M. S. Dresselhaus, G. Chen, M. Y. Tang, R. Yang, H. Lee, D. Wang, Z. Ren, J. P. Fleurial, and P. Gogna, Adv. Mater. (Weinheim, Ger.) **19**, 1043 (2007).
[5] L. D. Hicks and M. S. Dresselhaus, Phys. Rev. B **47**, 16631 (1993).
[6] R. Venkatasubramanian, E. Siivola, T. Colpitts, and B. O'Quinn, Nature (London) **413**, 597 (2001).
[7] T. C. Harman, P. J. Taylor, M. P. Walsh, and B. E. LaForge, Science **297**, 2229 (2002).
[8] T. Koga, S. B. Cronin, M. S. Dresselhaus, J. L. Liu, and K. L. Wang, Appl. Phys. Lett. **77**, 1490 (2000).
[9] J. P. Heremans, C. M. Thrush, and D. T. Morelli, J. Appl. Phys. **98**, 063703 (2005).
[10] K. F. Hsu, S. Loo, F. Guo, W. Chen, J. S. Dyck, C. Uher, T. Hogan, E. K. Polychroniadis, and M. G. Kanatzidis, Science **303**, 818 (2004).
[11] M. S. Dresselhaus, G. Chen, M. Y. Tang, R. G. Yang, H. Lee, D. Z. Wang, Z. F. Ren, J. P. Fleurial, and P. Gogna, in *Materials and Technologies for Direct Thermal to Electrical Energy Conversion*, edited by J. Yang, T. P. Hogan, R. Funakashi, and G. S. Nolas, MRS Symposia Proceedings No. 886 (Materials Research Society, Pittsburgh, 2006), p. 3.
[12] G. S. Nolas, J. Sharp, and H. J. Goldsmid, *Thermoelectrics: Basic Principles and New Materials Developments* (Springer, New York, 2001).
[13] Y. I. Ravich, in *CRC Handbook of Thermoelectrics*, edited by D. M. Rowe (CRC, New York, 1995), pp. 67–73.
[14] B. Moyzhes and V. Nemchinsky, Appl. Phys. Lett. **73**, 1895 (1998).
[15] K. Kishimoto and T. Koyanagi, J. Appl. Phys. **92**, 2544 (2002).
[16] J. P. Heremans, C. M. Thrush, and D. T. Morelli, Phys. Rev. B **70**, 115334 (2004).
[17] J. Martin, G. S. Nolas, W. Zhang, and L. Chen, Appl. Phys. Lett. **90**, 222112 (2007).
[18] W. Zhang, L. Zhang, Y. Cheng, Z. Hui, X. Zhang, Y. Xie, and Y. Qian, Mater. Res. Bull. **35**, 2009 (2000).
[19] J. Martin, G. S. Nolas, H. Wang, and J. Yang, J. Appl. Phys. **102**,

103719 (2007).
[20] Yu. I. Ravich, B. A. Efimova, and I. A. Smirnov, *Semiconducting Lead Chalcogenides* (Plenum, New York, 1970) (and references therein).
[21] W. Scanlon, *Solid State Physics* (Academic, New York, 1959), Vol. 9.
[22] C. Kittel, *Introduction to Solid State Physics*, 2nd ed. (Wiley, New York, 1956), p. 356.
[23] Z. H. Dughaish, Physica B **322**, 205 (2002).
[24] E. H. Putley, Proc. Phys. Soc. B **65**, 388 (1952).
[25] E. H. Putley, Proc. Phys. Soc. B **65**, 736 (1952).
[26] N. A. Poklonski, S. A. Vyrko, V. I. Yatskevich, and A. A. Kocherzhenko, J. Appl. Phys. **93**, 9749 (2003).
[27] J. Y. W. Seto, J. Appl. Phys. **46**, 5247 (1975).
[28] O. Vigil-Galan, Lıdice Vaillant, R. Mendoza-Perez, G. Contreras-Puente, J. Vidal-Larramendi, and A. Morales-Acevedo, J. Appl. Phys. **90**, 3427 (2001).
[29] G. Kiriakidis, M. Suchea, S. Christoulakis, and N. Katsarakis, Rev. Adv. Mater. Sci. **10**, 215 (2005).
[30] T. S. Zyubina, V. S. Neudachina, L. V. Yashina, and V. I. Shtanov, Surf. Sci. **574**, 52 (2005).
[31] R. Clasen, G. Harbeke, A. Krost, F. Levy, O. Madelung, K. Maschke, G. Nimtz, B. Schlicht, F. J. Schmitte, and J. Treusch, in *Semiconductors*, edited by K. H. Hellwege and O. Madelung, Landolt-Börnstein, New Series, Group III, Vol. 17, Pt. F (Springer, New York, 1983), p. 170.
[32] V. V. Mitin, Phys. Rev. B **31**, 2584 (1985).
[33] L. M. Rogers, Br. J. Appl. Phys. **1**, 1067 (1968).
[34] A. J. Crocker and L. M. Rogers, Br. J. Appl. Phys. **18**, 563 (1967).
[35] J. M. O. Zide, D. Vashaee, Z. X. Bian, G. Zeng, J. E. Bowers, A. Shakouri, and A. C. Gossard, Phys. Rev. B **74**, 205335 (2006).